PHOTONICS Research

Very large group delay in VHF band using coupled high temperature superconducting resonators

Tianning Zheng,[1] Bin Wei,[1,3] Fuchuan Lei,[2,4] and Bisong Cao[1]

[1]Department of Physics, State Key Laboratory Low-Dimensional Quantum Physics, Tsinghua University, Beijing 100084, China
[2]Department of Microtechnology and Nanoscience, Chalmers University of Technology, SE-41296 Gothenburg, Sweden
[3]e-mail: weibin@tsinghua.edu.cn
[4]e-mail: fuchuan@chalmers.se

Received 28 April 2021; revised 28 June 2021; accepted 25 July 2021; posted 26 July 2021 (Doc. ID 430185); published 8 September 2021

Storing a very high frequency (VHF) band (30–300 MHz) electromagnetic wave has many potential applications, such as phase modulation, buffering, and radio frequency memory. It can be effectively achieved by applying coupled resonator-based electromagnetically induced transparency (EIT) due to its slow light effect. However, the wavelength in the VHF band is too long to design resonators, and the group delay is limited by the high resistive loss of metal. The practical application of EIT in the VHF band is still a big challenge. In this work, we propose and experimentally demonstrate EIT response in a high-temperature superconducting (HTS) microwave circuit with coupled-resonator-induced transparency. The chip size of the HTS circuit is only 34 mm × 20 mm with a very low transparency frequency of 198.55 MHz. In addition, we implement very large group delay higher than 12.3 μs and 16.2 μs with working temperatures of 65 K and 50 K separately, which is much longer than the previous reported works on slow wave. The fabricated circuit is planar with working temperature about 65 K, and thus can be easily integrated into other microwave devices under the cryogenic conditions provided by a commercial portable Stirling cryocooler. Our proposed method paves a way for studying EIT in the microwave region due to the high quality factor of the HTS resonator, which has great potential use for radio-frequency memory in the future.

https://doi.org/10.1364/PRJ.430185

1. INTRODUCTION

Electromagnetically induced transparency (EIT) is a coherent phenomenon originally discovered in a three-level atomic system. A sharp transparent peak occurs in an absorption band due to the opposite phases of the two transition amplitudes canceling the absorption [1,2]. EIT and its mechanism have been widely demonstrated in many experimental systems, such as gas vapor atoms [3–6], cold atoms [7–9], metamaterials [10–17], photonic lattices [18–20], plasmons [21–24], superconductors [25–33], optomechanics [34,35], and coupled whispering-gallery-mode (WGM) resonators [36–39]. There is a sharp phase change within the narrow window accompanied by a large group delay. As a result, the group velocity of light is reduced, leading to important applications in slow-light devices [40]. In microwave region, EIT may be used in radio-frequency memory [41], an important technique for electronic warfare by storing the electromagnetic (EM) wave emitted from radar and transmitting it for jamming. The application in the very high frequency (VHF) band (30 to 300 MHz) has been widely demonstrated for its long detecting range; thus, radio-frequency memory based on EIT shows great potential in this microwave region. Coupled-resonator-induced transparency is a preferred choice for implementing EIT and storing the EM wave in the VHF band because the "atomic" levels can be designed by tuning the resonance frequency, loss, and coupling strength. Although EIT in the microwave region has been demonstrated in coupled metal resonators [42], their quality factor (Q) is relatively low, leading to low group delay. Previous works based on low-temperature superconductors can realize high-Q resonators [29], but they require an extremely low-temperature environment, typically below 10 K, which greatly limits their practical applications. In addition, previous works in low-temperature superconducting systems are mainly based on the theory of superconducting flux quantum circuit [25] or metamaterials [28]. As a result, their experimental systems are very complicated and hard to integrate with other microwave devices. Moreover, the wavelength is very large in the VHF band. Specifically, the wavelength will be 1.5 m when the frequency is 200 MHz in free space, which implies a very large size of resonators is required. The practical applications in radio-frequency memory of EIT in the VHF band are greatly limited and the convenient implementation of a large group delay is still a big challenge.

In this work, we propose and experimentally demonstrate EIT response in a microwave circuit with coupled high-temperature superconducting (HTS) resonators. Similar to coupled WGM resonators in the optical region, the circuit is designed with coupled HTS resonators, the Q of which can be very high, leading to a very large group delay. We introduce a spiral resonator to achieve a compact size at a very low microwave frequency of the VHF band. Furthermore, the fabricated circuit is planar, with a working temperature of about 65 K, and thus can be easily integrated to other microwave devices under the cryogenic conditions provided by a commercial portable Stirling cryocooler. Full-wave EM simulation is performed to illustrate the EIT, Fano resonances, and Autler–Townes splitting (ATS) phenomenon based on different central frequencies and coupling strength of the HTS resonators [43]. The circuit is then fabricated, and EIT is observed. After that, the group delay is measured at different temperatures.

2. DESIGN AND FABRICATION

Figure 1 shows the design, fabrication, and simulation results. Figure 1(a) displays the schematic diagram of an HTS microwave circuit, which is composed of a low-Q resonator, a high-Q resonator, and a feedline. Resonator 2 (R2) is the high-Q resonator, and resonator 1 (R1) is the low-Q resonator, which is achieved by using a transmission line coupling with the resonator at one end and connecting a 50 Ω impedance at the other end. The microwave signal is fed from the input port at the bottom end, and the output response is measured on the top end of the feed line. In the circuit, microwave travels as a quasi-transverse electric and magnetic (quasi-TEM) mode; thus, a surface current and voltage are converting to each other alternatively. Unlike the traveling-wave modes in the WGM resonator, the HTS resonator is a compact spiral resonator working at its fundamental frequency due to half-wavelength resonance. The center frequency of the resonator is 198.55 MHz. The dimensions as shown in the graph are only 34 mm × 20 mm, which amounts to $0.023\lambda_0 \times 0.013\lambda_0$, where λ_0 is the wavelength of the EM wave in free space.

The photograph of the fabricated sample is shown in Fig. 1(c). There are three steps to fabricate the proposed HTS device shown in Fig. 1(d). The circuit is fabricated on two separate MgO substrates with double-side coated YBCO HTS thin films. The electrical permittivity of MgO is more consistent throughout the whole layer than other substrates, such as Al_2O_3 and $LaAlO_3$ because MgO is isotropic in all directions. The fabrication involves photolithography with UV light as the first step. After that, ion-beam etching will be performed twice. Argon ions are used to etch the unwanted part in the gold layer and YBCO layer, leaving only the proposed structure. The gold layer is then removed by the ion-beam etching for the second time with a shorter time. Finally, the HTS circuit is then mounted on a metal carrier and is assembled into a shield box. A sapphire tuning screw is mounted on the top cover to correct the fabrication errors.

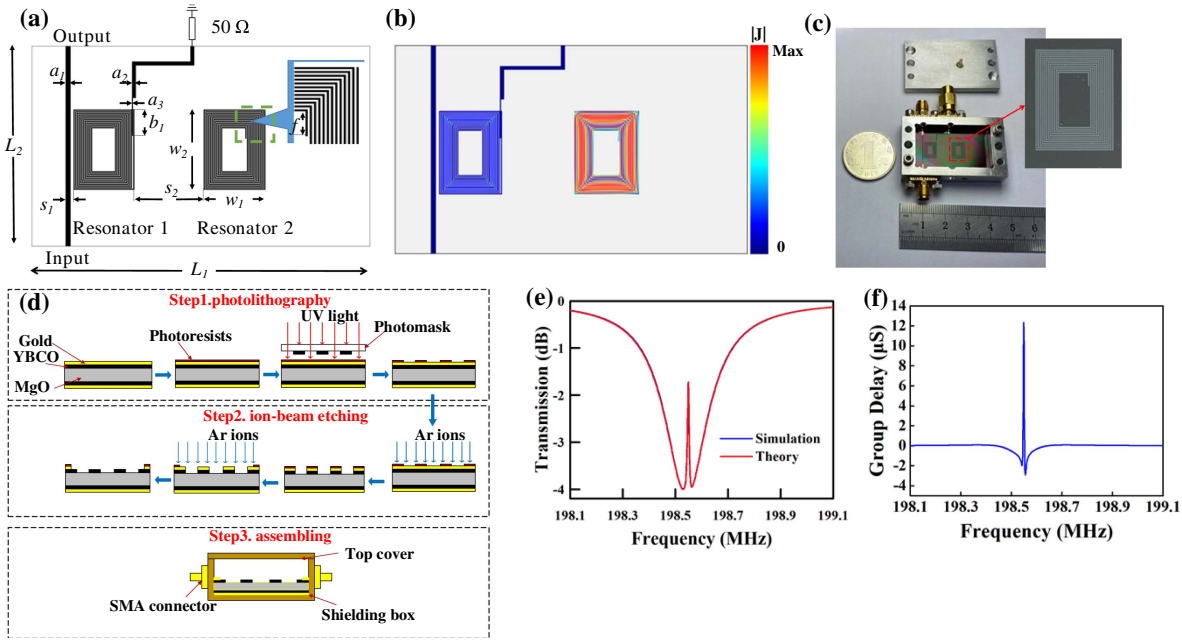

Fig. 1. Design, fabrication, and simulation results. (a) Schematic diagram of the HTS coupled resonator circuit; (b) simulated current density of the HTS coupled resonators' circuit at the transparent frequency; (c) photograph of the HTS coupled resonator circuit; (d) schematic diagram of fabrication process of the HTS circuit; (e) simulated and theoretical transmission spectra of the HTS coupled resonator circuit; (f) simulated group delay of the HTS coupled resonator circuit. The YBCO film has a conductivity of 1.2×10^{14} S/m and a thickness of 600 nm. The substrate is MgO with dimensions of 34 mm × 20 mm × 0.5 mm, and its relative permittivity is 9.7077. Due to the very low loss of the substrate, the loss tangent during simulation is set as 0, and the loss is equivalent to conductor loss. The depth of the air layer below the top cover is 5 mm. The dimensions in the circuit are as follows: $L_1 = 34$ mm, $L_2 = 20$ mm, $a_1 = 0.48$ mm, $a_2 = 0.36$ mm, $a_3 = 0.08$ mm, $b_1 = 2.56$ mm, $s_1 = 0.8$ mm, $s_2 = 7.2$ mm, $f = 1.20$ mm, $w_1 = 6.2$ mm, and $w_2 = 8$ mm. The number of turns of each spiral resonator is 12. The linewidth and line spacing are both 0.08 mm in the spiral resonators.

In the system depicted in Fig. 1(a), the output field is given as $A_{\text{out}} = A_p + \sqrt{\gamma_c}A_1$, where the field amplitude of R1 can be written as $A_1 = i\sqrt{\gamma_c}A_p\chi$ [43] with

$$\chi = \frac{\omega - (\omega_2 - i\gamma_2)}{\kappa^2 - [\omega - (\omega_1 - i\gamma_1)][\omega - (\omega_2 - i\gamma_2)]}, \quad (1)$$

where $\gamma_1 = \gamma_1' + \gamma_c$ and γ_2 denote the total losses in R1 and R2, respectively. γ_1' is the intrinsic loss of R1 and γ_c is the coupling loss between the feedline and R1. ω is the frequency of the probe microwave field A_p, while ω_1 and ω_2 denote the resonance frequencies of the two HTS resonators. κ is the coupling strength between the two HTS resonators. Then, the field transmission in decibels can be written as $T = 10\log|A_{\text{out}}/A_p|$.

In our experimental systems, the theoretically predicted parameters are shown as follows:

$$\omega_1 = 2\pi \times 198.5415 \text{ MHz},$$
$$\omega_2 = 2\pi \times 198.5500 \text{ MHz},$$
$$\gamma_1 = 2\pi \times 0.205000 \text{ MHz},$$
$$\gamma_2 = 2\pi \times 0.002900 \text{ MHz},$$
$$\gamma_c = 2\pi \times 0.040800 \text{ MHz},$$
$$\kappa = 2\pi \times 0.014000 \text{ MHz}.$$

The above theoretical model with the given parameters fits perfectly with the simulated transmission spectra, as shown in the Fig. 1(e). The results show a typical EIT response, that is, a very sharp peak appears in the center of an absorption band. Method of moments is used in the simulation with a cell size of 0.02 mm × 0.02 mm. The group delay is also simulated approximately, as shown in Fig. 1(f), and the simulated group delay is higher than 12.3 μs. This may be further increased by lowering the operating temperature. Figure 1(b) shows the current density distribution in the circuit, which demonstrates that energy is coupled to the high-Q resonator leading to its resonance at fundamental frequency because the current density is maximum at the center of the spiraled line and becomes minimum at the two ends of it.

3. RESULTS AND DISCUSSION

Coupled-resonator-induced transparency can achieve EIT, Fano resonances, and ATS based on different central frequencies and coupling strength [43]. If there is a significant difference between ω_1 and ω_2, Fano resonance will happen, while if ω_1 and ω_2 are approximately the same, EIT or ATS will happen, depending on the coupling strength κ. A threshold coupling strength κ_T to distinguish the transition between EIT and ATS is given by $2|\kappa_T| = (\gamma_1 - \gamma_2)/2$. When the system is in the strong coupling regime, $\kappa > \kappa_T$ and ATS will happen, while in the weak coupling regime, $\kappa < \kappa_T$, EIT will happen. Simulations are performed to demonstrate the three phenomena, as shown in Fig. 2. Separation of the two resonators s_2 is set to control the coupling strength between the two resonators, while length of the inner stub of the high-Q resonator f is set to tune the resonance frequency of R2.

As s_2 decreases, the coupling strength between the two resonators gets stronger. The sharp center in the transmission spectrum starts to broaden. After that, an ATS effect appears, as shown in Fig. 2(a). Simulations show that tuning f will alter the position of the sharp center, resulting in a Fano resonance. As shown in Fig. 2(b), when f is larger, the sharp center will be at a lower frequency. Meanwhile, the sharp center will be higher when f is smaller. The center frequency of the high-Q resonator is affected by the total length of the spiral line, as expected. For ATS, the group delay decreases dramatically due to the strong couplings, as shown in Fig. 2(c). However, when the coupling strength decreases, the group delay does not increase monotonously. A too weak coupling shows no benefit for achieving a very slow wave. The group delay of Fano resonance for each frequency is shown in Fig. 2(d). Fano resonance shows a violent sharp negative group delay and sharp positive group delay conversion, while EIT shows a very large positive group delay in the center but the negative group delay is relatively small. Among them, the group delay is the highest when EIT happens.

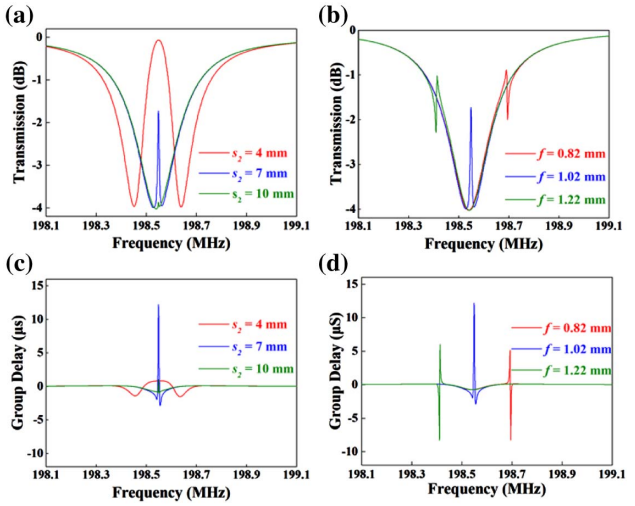

Fig. 2. Simulation study of EIT, ATS, and Fano resonance of the coupled resonators. (a) Simulated results of transmission spectra as s_2 varies, and f is set as 1.02 mm; (b) simulated results of transmission spectra as f varies, and s is set as 7.2 mm; (c) simulated corresponding group delay in (a); (d) simulated corresponding group delay in (b).

Figure 3(a) shows the schematic diagram of the measurement setup. The circuit is measured with an Agilent N5230C vector network analyzer with an input power of 0 dBm at 65 K. The cryogenic condition is provided by a commercial Stirling cryocooler with an output power of 6 W. The fabricated device is fixed on the cold head of the cryocooler in a vacuum chamber. The circuit is tuned with sapphire tuning screws on the top cover to correct fabrication errors, and the center frequency of the high-Q resonator is altered to achieve an EIT response. Before measurement, the network analyzer is calibrated using an electronic calibrator to cancel out the loss and phase difference between reference line 1 and reference line 2, as shown in Fig. 3(a). After that, the transmission spectra, phase difference, and group delay, which is caused by the HTS device under test, are measured in a range of frequency. The simulated and measured results of transmission spectra and group delays are shown in Fig. 3(b) and Fig. 3(c), respectively. The measured results are in good agreement with the simulation results.

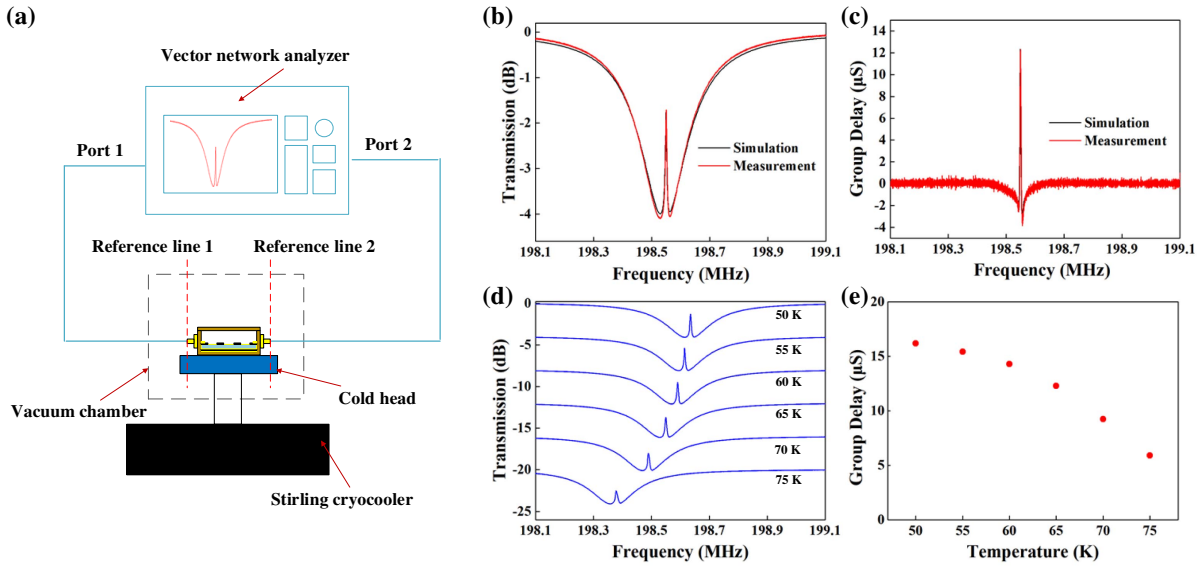

Fig. 3. Experimental setup and results. (a) Schematic diagram of the measurement setup; (b) comparison between simulation and measurement results of the transmission spectra of the HTS coupled resonator circuit; (c) comparison between simulation and measurement results of the group delay of the HTS coupled resonator circuit; (d) measured results of transmission spectra as temperature varies; (e) measured group delay at the transparent frequency as temperature varies.

The group delay is higher than 12.3 μs, which is much higher than the value previously reported. Moreover, the planar circuit is easy to be integrated, and the whole system, including the cryocooler, can be assembled as a portable device.

The conductivity of the HTS material strongly depends on the working temperature. The Q can be tuned by changing temperature, and the group delay of the circuit may be much larger. Figure 3(d) shows the temperature dependence of the transmission spectra. As the temperature decreases, the center frequency shifts slightly higher. The center frequency is 198.55 MHz at 65 K, and it shifts up to 198.64 MHz at 50 K while it shifts down to 198.38 MHz at 75 K. The group delay of the center frequency increases from 5.7 μs to 16.2 μs as the temperature decreases from 75 K to 50 K, as shown in Fig. 3(e). Lowering the temperature increases the group delay significantly, but a more severe working condition will be needed. In practical applications, the working temperature and performance of the device should be designed accordingly.

Table 1 shows some typical experimental systems implementing EIT in the microwave region. Some results only show the group delay, while the others only illustrate the group index. To compare the slow-wave properties clearly, we calculate the equivalent group index of our device with the following equation:

$$n_g = -\frac{c}{l}\frac{\partial\varphi}{\partial\omega}. \tag{2}$$

Here, c is the speed of light, l is the length of the transmission path, ω is the frequency, and φ is the phase of transmission. In our experiment, l is 20 mm, $\frac{\partial\varphi}{\partial\omega}$ is the group delay, with a number of 12 μs, and the equivalent group index is about 1.8×10^5. The group delay in this work is much larger than that of the method with traditional metal materials. In addition, the working temperature is much higher than that of the method with low-temperature superconductors. What is more, the circuit is a highly integrated device and can be conveniently connected to other microwave components.

4. CONCLUSION

In conclusion, we propose and experimentally demonstrate an EIT response in a microwave circuit with coupled HTS resonators. We implement very large group delay at the VHF band,

Table 1. Comparison of the EIT-Induced Maximum Group Delay or Index in Different Physical Systems[a]

Experimental System	Frequency (GHz)	Group Delay (ns)	Group Index	Working Temperature (K)
Metal-based metamaterial [17]	3	10		Room temperature
Coupled metal resonators [42]	1.5		530	Room temperature
Metal-superconductor hybrid metamaterial [28]	10.5	300		3
Coupled superconducting coplanar waveguide cavity and nanomechanical oscillator [29]	6	4×10^6		0.2
This work	0.2	1.2×10^4	1.8×10^5	65

[a]To just compare the order of magnitude as a conclusion, values in the table are approximated.

higher than 12.3 μs and 16.2 μs, with a working temperature of 65 K and 50 K, respectively. Simulated analysis of EIT, Fano resonances, and ATS shows EIT possesses the largest group delay, and this can be used for designing radio-frequency memory devices. Additionally, temperature-varying measurement shows the group delay increases significantly when the temperature is low. Our proposed method paves the way for studying EIT in the microwave region. Due to the high Q factor of the HTS resonator, the fabricated device shows great potential use for radio-frequency memory in the future.

Funding. National Natural Science Foundation of China (61371009).

Disclosures. The authors declare no conflicts of interest.

REFERENCES

1. S. E. Harris, J. E. Field, and A. Imamoğlu, "Nonlinear optical processes using electromagnetically induced transparency," Phys. Rev. Lett. **64**, 1107–1110 (1990).
2. K.-J. Boller, A. Imamoğlu, and S. E. Harris, "Observation of electromagnetically induced transparency," Phys. Rev. Lett. **66**, 2593–2596 (1991).
3. A. M. Akulshin, S. Barreiro, and A. Lezama, "Electromagnetically induced absorption and transparency due to resonant two-field excitation of quasidegenerate levels in Rb vapor," Phys. Rev. A **57**, 2996–3002 (1998).
4. M. D. Eisaman, A. André, F. Massou, M. Fleischhauer, A. S. Zibrov, and M. D. Lukin, "Electromagnetically induced transparency with tunable single-photon pulses," Nature **438**, 837–841 (2005).
5. M. Mücke, E. Figueroa, J. Bochmann, C. Hahn, K. Murr, S. Ritter, C. J. Villas-Boas, and G. Rempe, "Electromagnetically induced transparency with single atoms in a cavity," Nature **465**, 755–758 (2010).
6. R. Röhlsberger, H.-C. Wille, K. Schlage, and B. Sahoo, "Electromagnetically induced transparency with resonant nuclei in a cavity," Nature **482**, 199–203 (2012).
7. L. V. Hau, S. E. Harris, Z. Dutton, and C. H. Behroozi, "Light speed reduction to 17 meters per second in ultracold atomic gases," Nature **397**, 594–598 (1999).
8. G. Morigi, J. Eschner, and C. H. Keitel, "Ground state laser cooling using electromagnetically induced transparency," Phys. Rev. Lett. **85**, 4458–4461 (2000).
9. D. A. Braje, V. Balić, S. Goda, G. Y. Yin, and S. E. Harris, "Frequency mixing using electromagnetically induced transparency in cold atoms," Phys. Rev. Lett. **93**, 183601 (2004).
10. N. Papasimakis, V. A. Fedotov, N. I. Zheludev, and S. L. Prosvirnin, "Metamaterial analog of electromagnetically induced transparency," Phys. Rev. Lett. **101**, 253903 (2008).
11. P. Tassin, L. Zhang, T. Koschny, E. N. Economou, and C. M. Soukoulis, "Low-loss metamaterials based on classical electromagnetically induced transparency," Phys. Rev. Lett. **102**, 053901 (2009).
12. L. Zhang, P. Tassin, T. Koschny, C. Kurter, S. M. Anlage, and C. M. Soukoulis, "Large group delay in a microwave metamaterial analog of electromagnetically induced transparency," Appl. Phys. Lett. **97**, 241904 (2010).
13. J. Zhai, J. Zhou, L. Zhang, and W. Hong, "Behavioral modeling of power amplifiers with dynamic fuzzy neural networks," IEEE Microw. Wireless Compon. Lett. **20**, 528–530 (2010).
14. J. Gu, R. Singh, X. Liu, X. Zhang, Y. Ma, S. Zhang, S. A. Maier, Z. Tian, A. K. Azad, H. T. Chen, A. J. Taylor, J. Han, and W. Zhang, "Active control of electromagnetically induced transparency analogue in terahertz metamaterials," Nat. Commun. **3**, 1151 (2012).
15. P. Tassin, L. Zhang, R. Zhao, A. Jain, T. Koschny, and C. M. Soukoulis, "Electromagnetically induced transparency and absorption in metamaterials: the radiating two-oscillator model and its experimental confirmation," Phys. Rev. Lett. **109**, 187401 (2012).
16. Z. Vafapour, "Slow light modulator using semiconductor metamaterial," Proc. SPIE **10535**, 105352A (2018).
17. R. Yang, Q. Fu, Y. Fan, W. Cai, K. Qiu, W. Zhang, and F. Zhang, "Active control of EIT-like response in a symmetry-broken metasurface with orthogonal electric dipolar resonators," Photon. Res. **7**, 955–960 (2019).
18. Q. Xu, S. Sandhu, M. L. Povinelli, J. Shakya, S. Fan, and M. Lipson, "Experimental realization of an on-chip all-optical analogue to electromagnetically induced transparency," Phys. Rev. Lett. **96**, 123901 (2006).
19. Q. Xu, P. Dong, and M. Lipson, "Breaking the delay-bandwidth limit in a photonic structure," Nat. Phys. **3**, 406–410 (2007).
20. M. F. Limonov, M. V. Rybin, A. N. Poddubny, and Y. S. Kivshar, "Fano resonances in photonics," Nat. Photonics **11**, 543–554 (2017).
21. N. Liu, L. Langguth, T. Weiss, J. Kästel, M. Fleischhauer, T. Pfau, and H. Giessen, "Plasmonic analogue of electromagnetically induced transparency at the Drude damping limit," Nat. Mater. **8**, 758–762 (2009).
22. R. Taubert, M. Hentschel, J. Kästel, and H. Giessen, "Classical analog of electromagnetically induced absorption in plasmonics," Nano Lett. **12**, 1367–1371 (2012).
23. G. C. Dyer, G. R. Aizin, S. J. Allen, A. D. Grine, D. Bethke, J. L. Reno, and E. A. Shaner, "Induced transparency by coupling of Tamm and defect states in tunable terahertz plasmonic crystals," Nat. Photonics **7**, 925–930 (2013).
24. C. W. Hsu, B. G. DeLacy, S. G. Johnson, J. D. Joannopoulos, and M. Soljačić, "Theoretical criteria for scattering dark states in nanostructured particles," Nano Lett. **14**, 2783–2788 (2014).
25. A. A. Abdumalikov, O. Astafiev, A. M. Zagoskin, Y. A. Pashkin, Y. Nakamura, and J. S. Tsai, "Electromagnetically induced transparency on a single artificial atom," Phys. Rev. Lett. **104**, 193601 (2010).
26. P. M. Anisimov, J. P. Dowling, and B. C. Sanders, "Objectively discerning Autler-Townes splitting from electromagnetically induced transparency," Phys. Rev. Lett. **107**, 163604 (2011).
27. J. Wu, B. Jin, J. Wan, L. Liang, Y. Zhang, T. Jia, C. Cao, L. Kang, W. Xu, J. Chen, and P. Wu, "Superconducting terahertz metamaterials mimicking electromagnetically induced transparency," Appl. Phys. Lett. **99**, 161113 (2011).
28. C. Kurter, P. Tassin, L. Zhang, T. Koschny, A. P. Zhuravel, A. V. Ustinov, S. M. Anlage, and C. M. Soukoulis, "Classical analogue of electromagnetically induced transparency with a metal-superconductor hybrid metamaterial," Phys. Rev. Lett. **107**, 043901 (2011).
29. X. Zhou, F. Hocke, A. Schliesser, A. Marx, H. Huebl, R. Gross, and T. J. Kippenberg, "Slowing, advancing and switching of microwave signals using circuit nanoelectromechanics," Nat. Phys. **9**, 179–184 (2013).
30. O. Limaj, F. Giorgianni, A. Di Gaspare, V. Giliberti, G. De Marzi, P. Roy, M. Ortolani, X. Xi, D. Cunnane, and S. Lupi, "Superconductivity-induced transparency in terahertz metamaterials," ACS Photon. **1**, 570–575 (2014).
31. C. Zhang, J. Wu, B. Jin, X. Jia, L. Kang, W. Xu, H. Wang, J. Chen, M. Tonouchi, and P. Wu, "Tunable electromagnetically induced transparency from a superconducting terahertz metamaterial," Appl. Phys. Lett. **110**, 241105 (2017).
32. J. Joo, J. Bourassa, A. Blais, and B. C. Sanders, "Electromagnetically induced transparency with amplification in superconducting circuits," Phys. Rev. Lett. **105**, 073601 (2010).
33. Z. Vafapour, M. Dutta, and M. A. Stroscio, "Sensing, switching and modulating applications of a superconducting THz metamaterial," IEEE Sens. J. **21**, 15187–15195 (2021).
34. A. H. Safavi-Naeini, T. P. M. Alegre, J. Chan, M. Eichenfield, M. Winger, Q. Lin, J. T. Hill, D. E. Chang, and O. Painter, "Electromagnetically induced transparency and slow light with optomechanics," Nature **472**, 69–73 (2011).
35. H. Xiong and Y. Wu, "Fundamentals and applications of optomechanically induced transparency," Appl. Phys. Rev. **5**, 031305 (2018).
36. D. U. Smith, H. Chang, K. A. Fuller, A. T. Rosenberger, and R. W. Boyd, "Coupled-resonator-induced transparency," Phys. Rev. A **69**, 063804 (2004).
37. K. Totsuka, N. Kobayashi, and M. Tomita, "Slow light in coupled-resonator-induced transparency," Phys. Rev. Lett. **98**, 213904 (2007).

38. F.-C. Lei, M. Gao, C. Du, Q.-L. Jing, and G.-L. Long, "Three-pathway electromagnetically induced transparency in coupled-cavity optomechanical system," Opt. Express **23**, 11508–11517 (2015).
39. C. Wang, X. Jiang, G. Zhao, M. Zhang, C. W. Hsu, B. Peng, A. D. Stone, L. Jiang, and L. Yang, "Electromagnetically induced transparency at a chiral exceptional point," Nat. Phys. **16**, 334–340 (2020).
40. B. Wu, J. F. Hulbert, E. J. Lunt, K. Hurd, A. R. Hawkins, and H. Schmidt, "Slow light on a chip via atomic quantum state control," Nat. Photonics **4**, 776–779 (2010).
41. S. D. Berger, "The spectrum of a digital radio frequency memory linear range gate stealer electronic attack signal," in *Proceedings of the 2001 IEEE Radar Conference* (2001), pp. 27–30.
42. M. Amin, R. Ramzan, and O. Siddiqui, "Slow wave applications of electromagnetically induced transparency in microstrip resonator," Sci. Rep. **8**, 2357 (2018).
43. B. Peng, Ş. K. Özdemir, W. Chen, F. Nori, and L. Yang, "What is and what is not electromagnetically induced transparency in whispering-gallery microcavities," Nat. Commun. **5**, 5082 (2014).